




Added-mass force in dry granular matterA. Seguin  and P. Gondret *Université Paris-Saclay, CNRS, Laboratoire FAST, F-91405 Orsay, France* (Received 8 November 2021; revised 4 February 2022; accepted 6 May 2022; published 20 May 2022)

From two-dimensional (2D) numerical simulations of the motion of a circular intruder into a dry granular packing, we provide evidence for a specific force term in the case of unsteady motion in addition to the force corresponding to a steady motion. We show that this additional term is proportional to the acceleration of the intruder relative to the grains as the added-mass force known for simple fluids. This force term corresponds to a variation in the kinetic energy of the surrounding flow and is characterized by a coefficient C_{AM} which is intrinsically linked to the nature of the granular media. An analytical calculation of the added-mass coefficient C_{AM} is developed based on the specific velocity field known for 2D granular flow around a cylinder. The theoretical value is shown to depend on the grain-cylinder size ratio, in good agreement with the measurements from our unsteady simulations.

DOI: [10.1103/PhysRevE.105.054903](https://doi.org/10.1103/PhysRevE.105.054903)**I. INTRODUCTION**

Granular flow around obstacles has received much attention in recent years [1–12] and the drag force on moving objects is a key physical ingredient to be considered in numerous situations such as bio-inspired locomotion [13] or anchoring problems [14]. The rheological characteristics of flowing materials have a strong influence on the drag force, which can thus be very different for complex fluids, such as polymers, suspensions, foams, or granular materials with shear-thinning or shear-thickening behavior, when compared to simple Newtonian fluids [15]. The concept of added mass, which was introduced by Bessel to describe the motion of a pendulum in a fluid [16], is related to the work necessary to modify the kinetic energy of the surrounding fluid in the case of an unsteady motion with a velocity $U(t)$ varying with the time t . The pressure field is modified and induces an additional force term proportional to the acceleration dU/dt and to the mass ρV of fluid of density ρ which is displaced by the object of volume V , with a numerical prefactor C_{AM} that can be calculated analytically for simple shapes such as spheres ($C_{AM} = 1/2$) or cylinders ($C_{AM} = 1$) in perfect fluids [15,17]. These values are for isolated objects in a infinite fluid, but may be slightly modified by close boundaries [18].

In granular matter, even if unsteady flows arise in many situations, such as for impacts [5,6,19], locomotion [13], or anchoring [14] in sands, the models developed are, in general, based on a steady drag force only, except in situations where the surrounding fluid is not negligible such as sediment transport [20] and fluidized beds [21]. This force has been investigated in many experiments and numerical studies for objects of simple shapes such as cylinders [1,4,7–9] or spheres [11,12], or even more complex shapes [3]. At high velocity, the drag force scales as U^2 [4,10–12], as in the inertial hydrodynamic regime corresponding to large Reynolds number $Re = \rho U D / \eta$ for Newtonian fluids of viscosity η . But at

low velocity, the drag force is generally independent of U [1], in contrast with Newtonian fluids [15]. This is due to the fact that the effective “viscosity” of the grain assembly is decreased close to the object by the shear with a larger “granular temperature” [7]. In the case where external vibrations are applied to the granular matter, the drag force may display a linear dependence with U [22] as in viscous fluids at low Re [15]. As the viscosity is hard to define for granular matter and depends on pressure [23], the Froude number Fr is often used instead of Re to separate the different flow regimes. In the case of a granular layer of vertical height h in the gravity field g , $Fr = U / (gh)^{1/2}$ is indeed the pertinent parameter for the steady force regimes [24]. In granular matter, the added-mass force is sometimes mentioned to explain striking experimental results [25], but is still unknown. This force is expected to be different from Newtonian fluids due to its complex rheological behavior, which is still the aim of an intense research activities with jamming, yield stress, and shear thinning [26].

We show in this paper that an added-mass force arises for unsteady motion in granular matter. To put in light this force term, we consider a simple flow configuration where an intruder is moved within a granular layer, as sketched in Fig. 1. We perform two-dimensional (2D) simulations using a discrete element method (DEM) based on molecular dynamics, and calculate the instantaneous force exerted by the grains of diameter d on the circular intruder of diameter D . We show that a force peak arises when the intruder is accelerated. This force peak, proportional to acceleration, corresponds to an added-mass force term characterized by a coefficient C_{AM} which varies with the grain-cylinder size ratio d/D , i.e., C_{AM} is close to 1 for vanishing d/D but can be much larger than 1 for $d/D \gtrsim 0.1$. Using known velocity fields specific to granular matter, C_{AM} can be calculated analytically and is found to be in good agreement with the measurements from the unsteady simulations, showing the same variation with D/d .

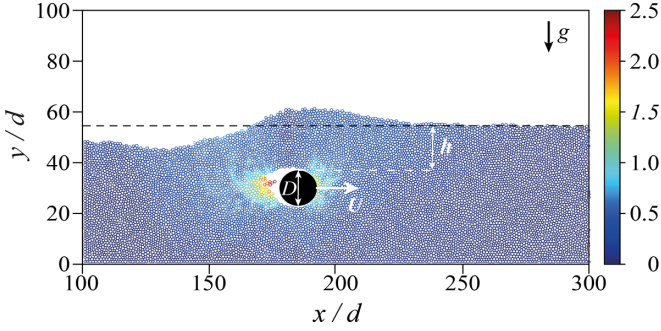


FIG. 1. Snapshot of the flow configuration. A large disk of diameter D is moved horizontally at an imposed velocity U along the x direction at the depth h of a two-dimensional layer of small grains of diameter d within the vertical gravity field g . The simulation parameters here are $U = 0.5$ m/s, $D = 15d$, and $h = 15.5d$ [$\text{Fr} = U/(gh)^{1/2} = 1.3$], with $d = 1$ mm grains colored according to their velocity u , from blue at $u = 0$ to dark red at $u/U = 2.5$.

II. NUMERICS

A molecular dynamic method is used to perform 2D simulations in a flow configuration, illustrated in Fig. 1, where a large disk of diameter D is moved at an imposed velocity U along the horizontal x direction at the depth h of a planar layer of smaller grains of diameter d . Such a technique has already been used to well reproduce unsteady situations such as impacts [5]. Most of our simulations have been performed with $D = 15d$ and a few with different D in the range $1 \leq D/d \leq 100$. The granular medium consists of spherical beads with a uniform size distribution between $0.8d$ and $1.2d$, where $d = 1$ mm is the mean diameter, to avoid any crystallization. Each grain has the same Young's modulus $E = 1$ GPa and the same mass m so that the grain density is distributed between $0.6\rho_g$ and $2\rho_g$ around its mean value $\rho_g \simeq 6.5m/\pi d^3$. The grain interactions f_{ij} between two grains come into play when the distance r_{ij} between two grains is smaller than $(d_i + d_j)/2$, with only normal component and no tangential component. The normal force is a dissipative Hertzian force of the form $f_{ij} = k\zeta^{3/2} - \lambda \frac{d\zeta}{dt}$, where $\zeta = (d_i + d_j)/2 - r_{ij}$ is the interpenetration of the grains, k the stiffness of the contact, and λ a damping coefficient. The stiffness k is directly related to the mechanical property and size of the grains through $k = E\sqrt{d}/2$. The damping coefficient λ is adjusted to reproduce a restitution coefficient $e_n = 0.5$ defined as the ratio of the normal velocities before and after a binary collision. The absence of a tangential component in the force contact model corresponds to no microscopic friction. However, a macroscopic friction arises from steric hindrance in the granular packing [27].

To prepare the initial state, the intruder was first fixed at a given initial position $(x_0, y_0) = (37.5d, 30d)$, where $y = 0$ corresponds to the bottom wall and $x = 0$ and $x = L$ correspond to the lateral walls of a container of length L . Then, a dilute granular medium of N grains of diameter d is placed above and let fall under the action of gravity ($g = 10 \text{ m s}^{-2}$ parallel to the y direction), which leads to a loose random packing up to a mean height $H \simeq 60d$, with a surface fraction $\phi = N\pi d^2/4HL \simeq 0.83$ less than the critical value $\phi_J = 0.85$

[28,29]. The effective density of the grain assembly is given by $\rho = 2\phi\rho_g/3$ as the grains are spherical. Once the initial configuration has been prepared, the intruder is moved horizontally at a velocity U along the x direction from $x = 0.1L$ to $x = 0.9L$. During the intruder motion, we record the drag force F . The time step is small enough to ensure numerical convergence and the length L of the container is large enough ($375d \leq L \leq 750d$) to avoid any influence of the lateral walls on the drag force [30].

III. STEADY MOTION

We first check the different force steady regimes depending on the Froude number. A typical instantaneous force signal $F(t)$ is shown in Fig. 2(a) for an imposed constant velocity $U = 0.5$ m/s corresponding to the Froude number $\text{Fr} = U/(gh)^{1/2} \simeq 1.3$. The drag force $F(t)$ exhibits strong and rapid fluctuations which may be associated to the formation and breakage of force chains [31,32]. When averaged over 10^5 successive points (time steps) corresponding to the displacement $\Delta x/D \simeq 0.2$, the drag force does not vary so much around the steady value $F_S \simeq 3.3\rho ghDd$ obtained by averaging over the entire time window corresponding the large relative displacement $\Delta x/D \simeq 6$. These observations are in agreement with experiments [33]. For different velocities U and thus different Fr , the steady force F_S is different, as reported in Fig. 2(b). A plateau is observed at low Fr , corresponding to the quasistatic regime where the force does not depend on velocity, i.e., $F_S = C_{Dqs}\rho ghDd$ with a quasistatic drag coefficient $C_{Dqs} \simeq 1$ for $\text{Fr} \ll 1$ (horizontal dashed line). The inertial regime at high Fr is also observed where the force increases with the square of the velocity, i.e., $F_S/(\rho ghDd) = 0.4\text{Fr}^2$ [dashed line of slope 2 in Fig. 2(b)] so that $F_S = C_{Di}\rho DdU^2/2$ with an inertial drag coefficient $C_{Di} \simeq 0.8$. The crossover between these two limit regimes is expected around $\text{Fr}_c = (2C_{Dqs}/C_{Di})^{1/2} \simeq 1.6$. Close to this crossover, the increase of F with Fr is approximately linear, i.e., $F_S/(\rho ghDd) \simeq 3.2\text{Fr} - 3.3$ in the range $2 \leq \text{Fr} \leq 6$, as shown in the inset of Fig. 2(b).

IV. UNSTEADY MOTION

We now consider an unsteady motion with a phase of constant acceleration Γ between two phases of constant velocities U_i and $U_f > U_i$. This acceleration is applied at the time $t = t_a$ during the time interval τ so that $\Gamma = dU/dt = (U_f - U_i)/\tau$. In the following, we change only the τ for changing the Γ . We choose the initial and final velocities in the range where the steady drag force increases linearly with velocity, i.e., $U_i = 1$ m/s and $U_f = 2$ m/s corresponding to the Froude numbers $\text{Fr}_i \simeq 2.6$ and $\text{Fr}_f = 5.1$, respectively, and to the steady forces $F_{S_i} \simeq 5\rho ghDd$ and $F_{S_f} \simeq 13\rho ghDd \simeq 2.6F_{S_i}$, respectively. During the unsteady motion, the force F is thus expected to increase linearly with time at low acceleration where no significant unsteady force term is expected, and an extra unsteady term F_{AM} is expected to arise at high acceleration. The time evolution of the force measured in the simulations is reported in Fig. 3 for three typical accelerations Γ from 8.3 m/s^2 ($0.9g$) to 250 m/s^2 ($25g$) with filtered signals so that the unsteady force term is expected to display a bell

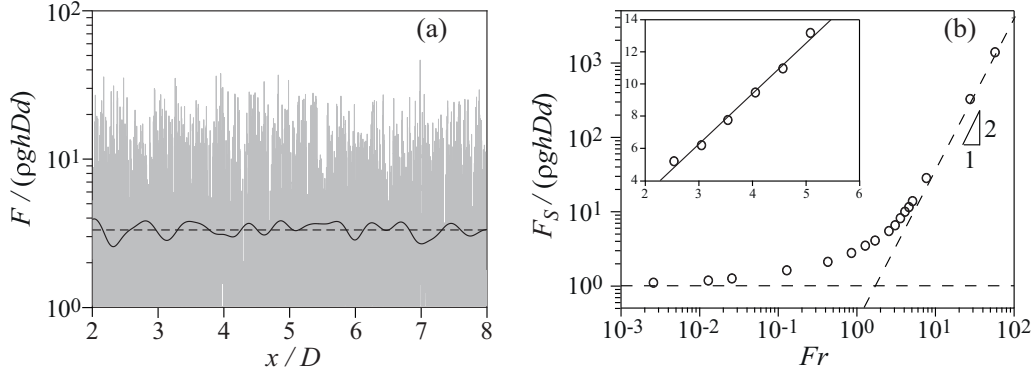


FIG. 2. (a) Dimensionless drag force $F/(\rho gh D d)$ as a function of the dimensionless time $tU/D = x/D$ for a disk of diameter $D = 15d$ moving with $U = 0.5 \text{ m/s} \simeq 1.3(gh)^{1/2}$ at the depth $h = 15.5d$ of a packing of grains of density $\rho = 10^3 \text{ kg m}^{-3}$. Solid line shows instantaneous force (in gray) and force averaged over 10^5 successive points (time step) corresponding here to $\Delta x/D = 0.2$ (in black). Dashed line shows mean value $F_S/(\rho gh D d) = 3.3$ over the entire time window ($\Delta x/D = 6$). (b) Dimensionless steady drag force $F_S/(\rho gh D d)$ as a function of the Froude number $Fr = U/\sqrt{gh}$ in a log-log plot for the whole range of Fr and (inset) in a lin-lin plot for a narrow range of Fr around 4. Circles show data from numerical simulations for an intruder disk of diameter $D = 15d$ moving at different constant velocities U and thus different Froude numbers $Fr = U/(gh)^{1/2}$, dashed line shows asymptotic behaviors with a constant plateau value $F_S/(\rho gh D d) = 1$ at $Fr \ll 1$ or a quadratic law $F_S/(\rho gh D d) = 0.4 Fr^2$ at $Fr \gg 1$, and solid line shows best linear fit $F_S/(\rho gh D d) = 3.2 Fr - 3.3$ in the range $2 \leq Fr \leq 6$.

shape. For the smallest acceleration ($\Gamma = 0.9g$), the force increases about linearly during the acceleration phase from F_{S_i} to F_{S_f} so that no extra unsteady force term can be clearly seen. For the largest acceleration ($\Gamma = 25g$), we observe a large force peak during the acceleration phase, which undoubtedly indicates an extra unsteady force term. For the intermediate acceleration ($\Gamma = 12.5g$), a smaller force peak can be seen during the unsteady motion. The calculation of the unsteady force is made by averaging the force signal $F(t)$ over the time interval τ corresponding to the constant acceleration Γ . The extra unsteady force term F_{AM} is then computed by withdrawing the steady force term $(F_{S_i} + F_{S_f})/2$ to the mean force $\langle F \rangle_\tau$ calculated from the instantaneous signal $F(t)$, i.e., $F_{AM} = \langle F \rangle_\tau - (F_{S_i} + F_{S_f})/2$. This extra unsteady term F_{AM} is reported in the inset of Fig. 4 as a function of $\rho V \Gamma$, both normalized by the initial steady force F_{S_i} . The data points

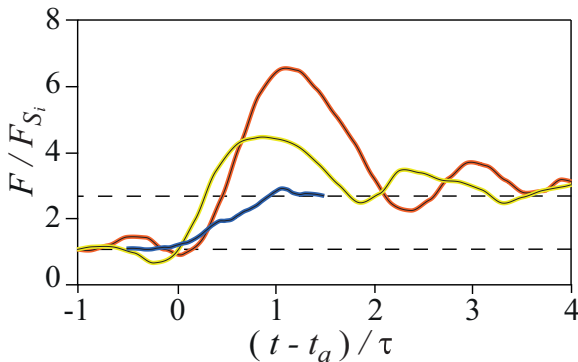


FIG. 3. Time evolution of the force $F(t)/F_{S_i}$ for a disk of diameter $D = 15d$ accelerating from $U_i = 1 \text{ m/s} \simeq 2.6(gh)^{1/2}$ to $U_f = 2 \text{ m/s} \simeq 5.1(gh)^{1/2}$, with $\Gamma = 0.9g$ (blue line), $12.5g$ (yellow line), and $25g$ (red line). The force signal is averaged over 10^5 successive points corresponding to $\tau/10$. Dashed lines show expected initial and final steady forces F_{S_i} and $F_{S_f} = 2.6F_{S_i}$.

made by varying the acceleration align well along a straight line of slope 1 in the log-log plot of Fig. 4, which means that the unsteady extra-force term F_{AM} is proportional to the acceleration of the intruder Γ . Note that the point obtained at the lowest Γ is not significant since the added-mass force is very small, i.e., only about 3% of the initial steady force F_{S_i} . Other points made by varying the grain density fall on the same master curve, meaning that F_{AM} is also proportional to the mass of grains displaced by the intruder of volume $V = \pi D^2/4$. All these findings demonstrate that F_{AM} corresponds to an added-mass force. A good linear fit of the data of Fig. 4

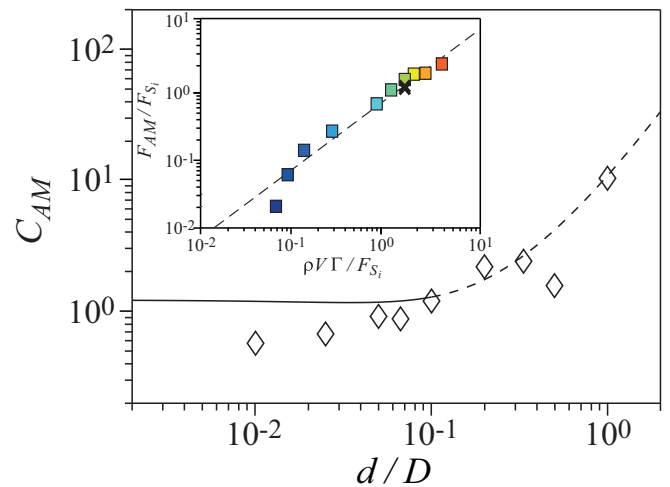


FIG. 4. Added-mass coefficient C_{AM} as a function of the grain-cylinder size ratio d/D . Diamonds show simulations results, and solid and dashed lines show the theoretical prediction from Eq. (1) with $\alpha = 1/4 + 2d/D$. Inset shows dimensionless unsteady force F_{AM}/F_{S_i} as a function of $\rho V \Gamma / F_{S_i}$ for $4 < \Gamma \leq 500 \text{ m s}^{-2}$, $D = 15d$, and $\rho = 10^3 \text{ kg m}^{-3}$ (\square), and for $\rho = 10^2 \text{ kg m}^{-3}$ and 10^4 kg m^{-3} (\times). Dashed line shows best linear fit $F_{AM} = 0.8 \rho V \Gamma$.

is obtained for $F_{AM} = (0.8 \pm 0.1)\rho V \Gamma$. This corresponds thus to the added-mass coefficient $C_{AM} = F_{AM}/\rho V \Gamma = 0.8 \pm 0.1$ close to the value 1 known for Newtonian fluids. By making simulations with other cylinder diameters D in the range $1 \leq D/d \leq 100$, we observe that the added-mass coefficient C_{AM} increases with d/D with a value slightly smaller than 1 for $d/D \lesssim 0.1$ but that becomes much larger than 1 above 0.1.

V. THEORETICAL MODELING

The rheology of granular media is quite different from Newtonian fluids [23,34,35] so that the flow of grains around an obstacle is quite specific. Several experimental studies have measured the velocity field of a stationary flow of grains around a cylinder in vertical penetration [7,8,36,37] and the unsteady velocity field in impact situations was found to be similar [38]. According to these studies, the velocity field \mathbf{u} of the grain flow around the cylinder can be approximately modeled as $\mathbf{u}(r, \theta)/U = A_r(r) \cos \theta \mathbf{e}_r + A_\theta(r) \sin \theta \mathbf{e}_\theta$, where r is the distance from the cylinder center and θ is the angle from the direction of motion. The radial functions A_r and A_θ for the radial and azimuthal velocities can be approximated by $A_r(r) = \exp[-(r - D/2)/\lambda]$ and $A_\theta(r) = (r/\lambda - 1) \exp[-(r - D/2)/\lambda]$, respectively [8]. The characteristic length λ has been shown to scale with the cylinder size with some effect of the grain size, i.e., $\lambda \simeq D/4 + 2d$ from measurements performed for $d/D \lesssim 0.1$ [8]. The exponential variation of the velocity field in granular matter is quite different from that in Newtonian fluids, which displays power-law variations. The added-mass coefficient C_{AM} which corresponds to a variation in the kinetic energy of the surrounding fluid can be calculated in the case of the 2D granular flow around a cylinder of diameter D as [39]

$$C_{AM} = \frac{4}{\pi D^2} \int_{r=D/2}^{+\infty} \int_{\theta=0}^{2\pi} \left[\frac{\mathbf{u}(r, \theta)}{U} \right]^2 r dr d\theta = \frac{1 - \alpha + 6\alpha^2 + 6\alpha^3}{4\alpha}, \quad (1)$$

where $\alpha = \lambda/D$. C_{AM} is a function of α only, whose value depends on the grain-cylinder size ratio d/D . With $\alpha = 1/4 +$

$2d/D$ taken from [8], Eq. (1) leads to $C_{AM} = 39/32 \simeq 1.2$ at vanishing d/D , which is close to the value 1 corresponding to Newtonian fluids even if the velocity field is quite different for granular matter. For increasing d/D , the C_{AM} value predicted by Eq. (1) increases and may be much larger for $d/D \gtrsim 0.1$ as shown in Fig. 4. These theoretical predictions are not far from the values given by the numerical simulations, and in particular they do explain the increase of C_{AM} with d/D by the increase of λ with d/D . Note that the theoretical C_{AM} values estimated here may be slightly modified by the precise flow configuration, as the near free surface parallel to the cylinder motion in the simulations.

VI. CONCLUSION

With force measurements from 2D numerical simulations of an intruder disk accelerating in granular matter, we highlight that an extra force term arises corresponding to an added-mass force. The added-mass coefficient C_{AM} depends on the specific velocity field of the granular flow around the cylindrical disk, which is known to display exponential variation with a characteristic length that increases with the grain/cylinder size ratio d/D [8], i.e., C_{AM} is close to one at low d/D and may be much larger for $d/D \gtrsim 0.1$. This can have important technical consequences to be taken into account in dimensioning equipments. With our findings, the added-mass force is expected to be larger than the steady drag force when $\Gamma > (4C_{Dqs}/\pi C_{AM})gh/D$ in the quasistatic regime or when $\Gamma > (2C_{Di}/\pi C_{AM})U^2/D$ in the inertial regime. With C_{Dqs} , C_{Di} , and C_{AM} all of the order of 1, this leads to the simple criteria $\Gamma \gtrsim gh/D$ or $\Gamma \gtrsim U^2/D$. Added mass could thus be important, especially at low depth or in low gravity environments, and at low velocity. This poses a milestone for forthcoming experimental investigations and 3D numerical simulations to be developed.

ACKNOWLEDGMENTS

We are grateful to B. Ndoye for technical support and B. Darbois Texier and M. Rabaud for fruitful discussions.

-
- [1] R. Albert, M. A. Pfeifer, A.-L. Barabási, and P. Schiffer, *Phys. Rev. Lett.* **82**, 205 (1999).
 - [2] I. Albert, P. Tegzes, B. Kahng, R. Albert, J. G. Sample, M. Pfeifer, A.-L. Barabási, T. Vicsek, and P. Schiffer, *Phys. Rev. Lett.* **84**, 5122 (2000).
 - [3] I. Albert, J. G. Sample, A. J. Morss, S. Rajagopalan, A.-L. Barabási, and P. Schiffer, *Phys. Rev. E* **64**, 061303 (2001).
 - [4] C. R. Wassgren, J. A. Cordova, R. Zenit, and A. Karion, *Phys. Fluids* **15**, 3318 (2003).
 - [5] M. P. Ciamarra, A. H. Lara, A. T. Lee, D. I. Goldman, I. Vishik, and H. L. Swinney, *Phys. Rev. Lett.* **92**, 194301 (2004).
 - [6] H. Katsuragi and D. J. Durian, *Nat. Phys.* **3**, 420 (2007).
 - [7] A. Seguin, Y. Bertho, P. Gondret, and J. Crassous, *Phys. Rev. Lett.* **107**, 048001 (2011).
 - [8] A. Seguin, Y. Bertho, F. Martinez, J. Crassous, and P. Gondret, *Phys. Rev. E* **87**, 012201 (2013).
 - [9] F. Guillard, Y. Forterre, and O. Pouliquen, *Phys. Rev. Lett.* **110**, 138303 (2013).
 - [10] J.-F. Boudet and H. Kellay, *Phys. Rev. Lett.* **105**, 104501 (2010).
 - [11] Y. Takehara, S. Fujimoto, and K. Okumura, *Europhys. Lett.* **92**, 44003 (2010).
 - [12] Y. Takehara and K. Okumura, *Phys. Rev. Lett.* **112**, 148001 (2014).
 - [13] R. D. Maladen, Y. Ding, C. Li, and D. I. Goldman, *Science* **325**, 314 (2009).
 - [14] S. Athani and P. Rognon, *Phys. Rev. Fluids* **4**, 124302 (2019).
 - [15] E. Guyon, J.-P. Hulin, L. Petit, and C. D. Matescu, *Physical Hydrodynamics* (Oxford University Press, Oxford, 2015).

- [16] G. G. Stokes, *Trans. Cambridge Philos. Soc.* **9**, 8 (1851).
- [17] A. R. Paterson, *A First Course in Fluid Dynamics* (Cambridge University Press, Cambridge, 1983).
- [18] L. M. Milne-Thomson, *Theoretical Hydrodynamics* (Dover, New York, 1996).
- [19] A. Seguin, Y. Bertho, P. Gondret, and J. Crassous, *Europhys. Lett.* **88**, 44002 (2009).
- [20] T. Pähz, E. J. R. Parteli, J. F. Kok, and H. J. Herrmann, *Phys. Rev. E* **89**, 052213 (2014).
- [21] D. Lohse, R. Rauhe, R. Bergmann, and D. Van Der Meer, *Nature (London)* **432**, 689 (2004).
- [22] A. Seguin and P. Gondret, *Phys. Rev. E* **96**, 032905 (2017).
- [23] P. Jop, Y. Forterre, and O. Pouliquen, *Nature (London)* **441**, 727 (2006).
- [24] T. Faug, *Eur. Phys. J. E* **38**, 34 (2015).
- [25] H. Katsuragi and D. J. Durian, *Phys. Rev. E* **87**, 052208 (2013).
- [26] B. Andreotti, Y. Forterre, and O. Pouliquen, *Granular Media: Between Fluid and Solid* (Cambridge University Press, Cambridge, 2013).
- [27] P.-E. Peyneau and J.-N. Roux, *Phys. Rev. E* **78**, 011307 (2008).
- [28] C. S. O'Hern, S. A. Langer, A. J. Liu, and S. R. Nagel, *Phys. Rev. Lett.* **88**, 075507 (2002).
- [29] C. S. O'Hern, L. E. Silbert, A. J. Liu, and S. R. Nagel, *Phys. Rev. E* **68**, 011306 (2003).
- [30] A. Seguin, Y. Bertho, and P. Gondret, *Phys. Rev. E* **78**, 010301(R) (2008).
- [31] A. H. Clark, L. Kondic, and R. P. Behringer, *Phys. Rev. Lett.* **109**, 238302 (2012).
- [32] A. H. Clark, A. J. Petersen, L. Kondic, and R. P. Behringer, *Phys. Rev. Lett.* **114**, 144502 (2015).
- [33] A. Seguin, C. Coulais, F. Martinez, Y. Bertho, and P. Gondret, *Phys. Rev. E* **93**, 012904 (2016).
- [34] M. Bouzid, M. Trulsson, P. Claudin, E. Clément, and B. Andreotti, *Phys. Rev. Lett.* **111**, 238301 (2013).
- [35] D. L. Henann and K. Kamrin, *Phys. Rev. Lett.* **113**, 178001 (2014).
- [36] E. Kolb, P. Cixous, N. Gaudouen, and T. Darnige, *Phys. Rev. E* **87**, 032207 (2013).
- [37] E. Kolb, P. Cixous, and J. Charmet, *Granular Matter* **16**, 223 (2014).
- [38] A. H. Clark, L. Kondic, and R. P. Behringer, *Phys. Rev. E* **93**, 050901(R) (2016).
- [39] C. E. Brennen, *A Review of Added Mass and Fluid Inertial Forces*, Report No. CR 82.010 (Naval Civil Engineering Laboratory, Port Hueneme, CA, 1982).